Image Reconstruction for High-Sensitivity Imaging by Using Combined Long/Short Exposure Type Single-Chip Image Sensor

Sanzo Ugawa, Takeo Azuma, Taro Imagawa, and Yusuke Okada

Advanced Tecnology Reserch Laboratories, Panasonic Corporation,
3-4 Hikaridai, Seika-cho, Sagara-gun, Kyoto 619-0237, Japan
ugawa.sanzo@jp.panasonic.com

Abstract. We propose a image reconstruction method and a sensor for high-sensitivity imaging using long-term exposed green pixels over several frames. As a result of extending the exposure time of green pixels, motion blur increases. We use motion information detected from high-frame-rate red and blue pixels to remove the motion blur. To implement this method, both long- and short-term exposed pixels are arranged in a checkerboard pattern on a single-chip image sensor. Using the proposed method, we improved fourfold the sensitivity of the green pixels without any motion blur.

1 Introduction

Recently, in the field of video input, the number of pixels has been continuously increasing while the pixel pitch has been decreasing. As pixels continue to shrink, the amount of light that can be received within a certain exposure time is reduced. Consequently, securing a higher Signal-to-Noise-Ratio (SNR) is becoming difficult.

To improve the SNR in the field of image sensing, technologies such as on-chip microlens [15] and back side illumination [12, 19] have been proposed. With the former, an on-chip microlens is structured on each pixel to focus incident light on a photodiode. This method triples the sensitivity. With the latter, the image sensor of back side illumination is wired under the transistor. The development of a sensor with a pixel size of 1.4 um that provides twice the sensitivity of conventional sensors has been reported [17, 21]. Also, the use of a sensor with a white pixel in the color filter area was proposed [11, 14].

For high resolution imaging using a small sensor, long-term exposure can increase the amount of incident light. However, motion blur occurs if the object of the image moves. The use of a combination approach with multiple images to reduce space-invariant blur has also been proposed [5, 6, 16, 18, 22]. Recently, a coded sampling method was proposed [3]. However, these methods cannot be used in small cameras because they require a number of image sensors.

We propose a image reconstruction algorithm and its dedicated sensor shown in Figure 1. The sensing method can effectively input a lot of light and motion

R. Kimmel, R. Klette, and A. Sugimoto (Eds.): ACCV 2010, Part III, LNCS 6494, pp. 641–652, 2011.

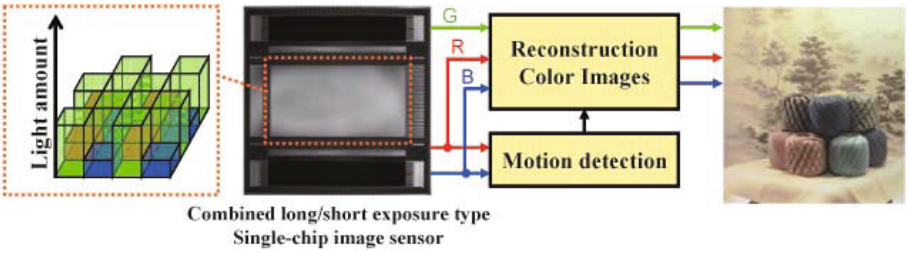

Fig. 1. With the proposed method images of G are obtained by long-term exposure. Motion blur of G is reduced by the pixel values of R and B in image processing.

information by mixing both long- and short-term exposed pixels on a single sensor. Additionally, we arranged the RGB on the basis of both human vision system and color correlation along the spectra of natural scenes.

The rest of the paper is as follows: We propose combined long/short exposure type image sensing in Section 2 and the reconstruction algorithm in Section 3. The results of experiments are shown in Section 4. We discuss the results in Section 5 and conclude the paper in Section 6.

2 Use of Single-Chip Image Sensor for Combined Long/Short Exposure Type Image Sensing

To improve the sensitivity and high-resolution imaging of a single-chip image sensor, our sensing method uses a long exposure time for some of the pixels on a single-chip image sensor. In this chapter, we explain the arrangement of both long- and short-term exposed pixels and the arrangement of RGB color filters in a single-chip image sensor.

2.1 Arrangement of Long-Term and Short-Term Exposed Pixels

In high-resolution imaging with a small image sensor, a long-term exposure is necessary to get the required amount of light. There is a trade-off relationship between the intervals of the exposure time and the frame-rate. Therefore, a long-term exposure decreases the frame-rate, and the captured image often includes motion blur if the object moves. However, this motion blur can be removed with motion information, so we then simultaneously take high-frame-rate images to obtain motion information.

In the image sensor, the difference between long- and short-term exposed images is the frame-rate. We define pixels which have a low-frame-rate image exposed over a long-term as 'long-term exposed pixels' and pixels which have a high-frame-rate image exposed over a short-term as 'short-term exposed pixels'.

We arranged a combination of both long-term exposed pixels and short-term exposed pixels in a single sensor. We also considered how to arrange each pixel for monochrome imaging. To efficiently estimate the motion information of

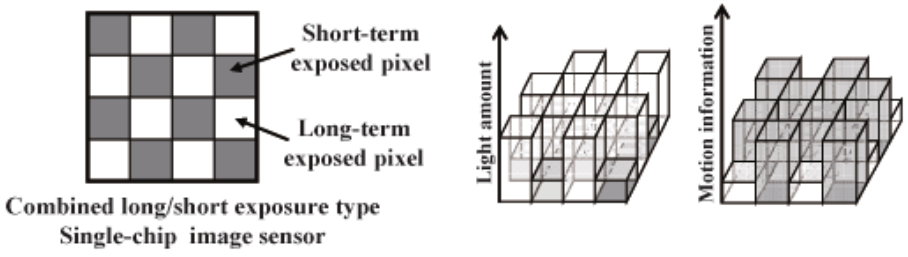

Fig. 2. Long- and short-term exposed pixels as checkerboard pattern in single-chip image sensor

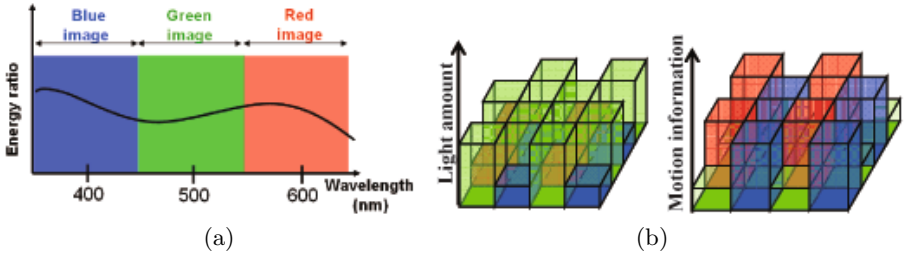

Fig. 3. (a) In the light spectrum, G is adjacent to B and R. (b) We arrayed G to long-term exposed pixels and R and B to short-term exposed ones.

long-term exposed pixels, the arrangement of short-term exposed pixels is homogeneously distributed. As shown in Figure 2, we arranged the pixels in a checkerboard pattern.

2.2 Arrangement of RGB Color Filters

We arranged RGB color filters in the sensor to reconstruct color images.

In the human vision system, spatial resolution for luminance is higher than that for hue, so we assigned green, which is the main factor in luminance, to the high-resolution image.

As shown in Figure 3(a), in the power spectrum of natural scenes, the power distribution of RGB are broad. The color of the adjoining wavelength has a high correlation. Both G-R and G-B are highly correlated. Hence, motion blur of G can be removed by using motion information calculated from R and B.

Based on both the properties of the human vision system and the color correlation among the spectra of natural scenes, we assigned G for long-term exposures and both R and B for short-term exposures, as illustrated in Figure 3(b). The motion information is detected from the R and B images because they have a high-frame-rate. This color arrangement is the same as that of the Bayer color arrangement [4].

3 Reconstruction of Color Images

We reconstructed color images from the sensing images explained in Section 2. The color images are calculated by minimizing a cost function. The cost function is composed of a difference between the ideal image and the sensing image with some regularization terms. In this section, we explain the cost function and how it can be solved by minimizing it.

3.1 Cost Function

Our method reconstructs color images by making use of the cost function. We define the ideal solution of RGB images as $\mathbf{f}$ and RGB sensed images as $\mathbf{g}_{\mathrm{R}}$, $\mathbf{g}_{\mathrm{G}}$, and $\mathbf{g}_{\mathrm{B}}$. $\mathbf{f}$ is a three-dimensional vector of R, G, and B and includes all RGB pixel values. Additionally, $\mathbf{f}$ includes R, G, and B values for each pixel position. The frame-rate of $\mathbf{f}$ is the same as the R/B, and the resolution of $\mathbf{f}$ is the same as the total number of pixels in a single sensor. The relation between $\mathbf{f}$ and the sensing RGB images, $\mathbf{g}_{\mathrm{R}}$, $\mathbf{g}_{\mathrm{G}}$, and $\mathbf{g}_{\mathrm{B}}$ is shown in Equation (1).

$$\begin{aligned} \mathbf{g}_{\mathrm{R}} &= \mathbf{H}_{\mathrm{R}}\mathbf{f} \\ \mathbf{g}_{\mathrm{G}} &= \mathbf{H}_{\mathrm{L}}\mathbf{H}_{\mathrm{G}}\mathbf{f} \\ \mathbf{g}_{\mathrm{B}} &= \mathbf{H}_{\mathrm{B}}\mathbf{f} \end{aligned} \tag{1}$$

As shown in Figure 2, $\mathbf{H}_{\mathrm{G}}$, $\mathbf{H}_{\mathrm{R}}$, and $\mathbf{H}_{\mathrm{B}}$ are degradation operators of G, R, and B pixel values in a Bayer pattern from the full pixel values, and $\mathbf{H}_{\mathrm{L}}$ is the degradation in frame-rate, which indicates long-term exposure. Equation (1) is a linear operation.

There are many candidates of $\mathbf{f}$ values that satisfy Equation (1). We add two regularization terms, $\mathbf{Q}_{\mathrm{S}}\mathbf{f}$ and $\mathbf{Q}_{\mathrm{m}}\mathbf{f}$, to specify $\mathbf{f}$. The terms $\mathbf{Q}_{\mathrm{S}}\mathbf{f}$ and $\mathbf{Q}_{\mathrm{m}}\mathbf{f}$ are based on the features of objects. The spatial smoothness can be given by $\mathbf{Q}_{\mathrm{S}}\mathbf{f}$, and the consistency of pixel value by the motion of the object can be given by $\mathbf{Q}_{\mathrm{m}}\mathbf{f}$. The cost function J that demands $\mathbf{f}$ is shown in Equation (2).

$$\begin{aligned} J = &||\mathbf{H}_{\mathrm{L}}\mathbf{H}_{\mathrm{G}}\mathbf{f} - \mathbf{g}_{\mathrm{G}}||^2 + ||\mathbf{H}_{\mathrm{R}}\mathbf{f} - \mathbf{g}_{\mathrm{R}}||^2 + ||\mathbf{H}_{\mathrm{B}}\mathbf{f} - \mathbf{g}_{\mathrm{B}}||^2 \\ &+ \lambda_{\mathrm{S}}||\mathbf{Q}_{\mathrm{S}}\mathbf{H}_{\mathrm{C}}\mathbf{f}||^2 + \lambda_{\mathrm{m}}||\mathbf{Q}_{\mathrm{m}}\mathbf{f}||^2 \end{aligned} \tag{2}$$

where λ_{S} and λ_{m} are regularization parameters. A detailed explanation of $\mathbf{Q}_{\mathrm{S}}\mathbf{f}$ and $\mathbf{Q}_{\mathrm{m}}\mathbf{f}$ is shown in the following subsection.

Color constraint term. $\mathbf{g}_{\mathrm{G}}$ is high resolution. Meanwhile, $\mathbf{g}_{\mathrm{R}}$ and $\mathbf{g}_{\mathrm{B}}$ are low resolution. When $\mathbf{g}_{\mathrm{G}}$ is spatially correlated with $\mathbf{g}_{\mathrm{R}}$ and $\mathbf{g}_{\mathrm{B}}$, the resolution of $\mathbf{g}_{\mathrm{R}}$ and $\mathbf{g}_{\mathrm{B}}$ can be improved by means of the correlation. On this point, we assume inter-RGB correlations to combine multiple color-channel images and implement them into the cost function as spatial color-smoothness. In natural images, the spatial smoothness differs depending on the basis of color space, we choose principal component vectors to define smoothness in order to set smoothness parameters effectively. The fourth and fifth terms in Equation (2)

are regularization terms that represent the spatial smoothness of the principal color of a reconstructed image sequence. First, the basis of the principal color space is defined by the principal component analysis of the RGB pixel values of natural images. Next, the principal color images are obtained by transformation matrices as follows:

$$\mathbf{f}_{\mathrm{C}i} = \mathbf{H}_{\mathrm{C}i}\mathbf{f}, i \in \{1, 2, 3\} \tag{3}$$

where $\mathbf{f}_{\mathrm{C}1}$, $\mathbf{f}_{\mathrm{C}2}$, and $\mathbf{f}_{\mathrm{C}3}$ represent the first, second, and third PCA color component images. The spatial smoothness of the pixel value in the principal-color image sequence is obtained by using $\mathbf{Q}_{\mathrm{S}}$ as a Laplacian operator. Here, we suppose that the pixel value varies smoothly in many regions in the reconstructed image, and the sum of squares of the second differentiation centered on each pixel is shown in Equation (4).

$$||\mathbf{Q}_{\mathrm{S}}\mathbf{H}_{\mathrm{C}}\mathbf{f}||^2 = \sum_{x=1}^{H}\sum_{y=1}^{W}\Big\{\frac{\partial^2}{\partial x^2}\mathbf{f}_{\mathrm{C}i}(x,y,z) + \frac{\partial^2}{\partial y^2}\mathbf{f}_{\mathrm{C}i}(x,y,z)\Big\}, i \in 1, 2, 3 \tag{4}$$

where H is the height of the image and W is the width of the image. The difference formulation of Equation (4) is shown in Equation (5).

$$\begin{aligned}||\mathbf{Q}_{\mathrm{S}}\mathbf{H}_{\mathrm{C}}\mathbf{f}||^2 = \sum_{x=1}^{H}\sum_{y=1}^{W}\Big\{&4\mathbf{f}_{\mathrm{C}i}(x,y,t) - \mathbf{f}_{\mathrm{C}i}(x-1,y,t) - \mathbf{f}_{\mathrm{C}i}(x,y-1,t)\\ &-\mathbf{f}_{\mathrm{C}i}(x+1,y,t) - \mathbf{f}_{\mathrm{C}i}(x,y+1,t)\Big\}, i \in 1, 2, 3\end{aligned} \tag{5}$$

Motion consistency term. We assume when an object moves, the pixel value does not change from the start to the end position. Motion information is detected by a sequence of three R/B color images, which are respectively captured at time t-1, t, and t+1. The relation of the time t-1 image and the time t image shows the motion toward the past, which is defined as (u_P,v_P). The relation of the time t image and the time t+1 image shows the motion toward the future, which is defined as (u_F,v_F). Motion information (u_P,v_P) and (u_F,v_F) are calculated as shown in Equation (6).

$$\begin{aligned}&\min_{u_P,v_P}\sum_{i=1}^{S_H}\sum_{j=1}^{S_W}|\mathbf{f}(x+i-u, y+j-v, t-1) - \mathbf{f}(x+i, y+j, t)|\\ &\min_{u_F,v_F}\sum_{i=1}^{S_H}\sum_{j=1}^{S_W}|\mathbf{f}(x+i-u, y+j-v, t+1) - \mathbf{f}(x+i, y+j, t)|\end{aligned} \tag{6}$$

S_H and S_W indicate a window size for motion detection. Pixel locations that correspond to G pixels in a Bayer pattern array are linearly interpolated by the surrounding R and B pixels to detect motion information at such pixels in advance. The regularization term regarding motion information is shown in Equation (7).

$$||Q_m f||^2 = \sum_{x=1}^{H}\sum_{y=1}^{W}\Big\{\mathbf{f}(x,y,t) - \mathbf{f}(x+u_P, y+v_P, t-1)\Big\}^2 + \sum_{x=1}^{H}\sum_{y=1}^{W}\Big\{\mathbf{f}(x,y,t) - \mathbf{f}(x+u_F, y+v_F, t+1)\Big\}^2 \tag{7}$$

We estimate sub-pixel motion by calculating the equiangular line fitting with the sum of absolute differences.

3.2 Minimization of the Cost Function

The output image $\mathbf{f}$ is obtained by minimizing the cost function J. Since J is the second form of $\mathbf{f}$, minimization of J always yields the global minimum of J. Thus, we can obtain $\mathbf{f}$ by differentiating J with respect to $\mathbf{f}$ and equating it with 0, as shown in Equation (8).

$$\begin{aligned}\frac{\partial J}{\partial \mathbf{f}} &= (\mathbf{H}_{\mathrm{L}}\mathbf{H}_{\mathrm{G}})^{\mathrm{T}}(\mathbf{H}_{\mathrm{L}}\mathbf{H}_{\mathrm{G}}\mathbf{f} - \mathbf{g}_{\mathrm{G}}) + \mathbf{H}_{\mathrm{R}}^{\mathrm{T}}(\mathbf{H}_{\mathrm{R}}\mathbf{f} - \mathbf{g}_{\mathrm{R}}) + \mathbf{H}_{\mathrm{B}}^{\mathrm{T}}(\mathbf{H}_{\mathrm{B}}\mathbf{f} - \mathbf{g}_{\mathrm{B}}) \\ &\quad + \sum_{i=1}^{3}\lambda_{\mathrm{C}i}(\mathbf{Q}_{\mathrm{S}}\mathbf{H}_{\mathrm{C}i})^{\mathrm{T}}\mathbf{Q}_{\mathrm{S}}\mathbf{H}_{\mathrm{C}i}\mathbf{f} + \lambda_{\mathrm{m}}\mathbf{Q}_{\mathrm{m}}^{\mathrm{T}}\mathbf{Q}_{\mathrm{m}}\mathbf{f} \\ &= 0\end{aligned} \tag{8}$$

Thus,

$$\begin{aligned}&\Big\{(\mathbf{H}_{\mathrm{L}}\mathbf{H}_{\mathrm{G}})^{\mathrm{T}}(\mathbf{H}_{\mathrm{L}}\mathbf{H}_{\mathrm{G}}) + \mathbf{H}_{\mathrm{R}}^{\mathrm{T}}\mathbf{H}_{\mathrm{R}} + \mathbf{H}_{\mathrm{B}}^{\mathrm{T}}\mathbf{H}_{\mathrm{B}} \\ &\quad + \sum_{i=1}^{3}\lambda_{\mathrm{C}i}(\mathbf{Q}_{\mathrm{S}}\mathbf{H}_{\mathrm{C}i})^{\mathrm{T}}\mathbf{Q}_{\mathrm{S}}\mathbf{H}_{\mathrm{C}i} + \lambda_{\mathrm{m}}\mathbf{Q}_{\mathrm{m}}^{\mathrm{T}}\mathbf{Q}_{\mathrm{m}}\Big\}\mathbf{f} \\ &\qquad = \Big\{(\mathbf{H}_{\mathrm{L}}\mathbf{H}_{\mathrm{G}})^{\mathrm{T}}\mathbf{g}_{\mathrm{G}} + \mathbf{H}_{\mathrm{R}}^{\mathrm{T}}\mathbf{g}_{\mathrm{R}} + \mathbf{H}_{\mathrm{B}}^{\mathrm{T}}\mathbf{g}_{\mathrm{B}}\Big\}\end{aligned} \tag{9}$$

Equation (9) can be solved by the conjugate gradient method.

4 Experimental Results

In this Section, we describe our simulation experiments. Additionally, we show how the developed image sensor is used and demonstrate that our method is effective.

4.1 Simulation

Our method was found to be effective even under low illumination. We used Peak-Signal-to-Noise-Ratio (PSNR) for evaluation. PSNR is calculated as follows:

$$PSNR(\mathbf{f}_{calc}) = 20\log_{10}\frac{S}{\sqrt{\frac{1}{N}||\mathbf{f}_{true}(x,y,t) - \mathbf{f}_{calc}(x,y,t)||^2}} \tag{10}$$

Table 1. Experimental conditions

Item	Parametaer
Number of scenes	20
Number of frames for each scene	180 frames
Interval of long-term exposure	4 frames
Noise level	8.06 (PSNR=30.0dB)

Table 2. Results of PSNR for Bayer reconstruction and proposed method

	Scene	1	2	3	4	5	6	7	8
Bayer reconstruction	R	30.71	30.71	28.85	28.81	27.12	30.03	27.48	23.48
	G	30.37	30.13	29.48	29.82	29.13	31.21	29.35	25.92
	B	30.79	29.97	28.87	28.89	27.65	30.01	28.57	23.38
	RGB	30.62	29.79	29.06	29.15	27.89	30.08	28.40	24.11
Proposed method	R	32.42	30.56	29.96	31.27	30.00	31.72	28.20	25.38
	G	33.14	31.38	30.83	31.95	31.39	32.81	29.90	26.11
	B	32.79	31.45	30.19	31.67	30.80	32.01	29.95	25.27
	RGB	32.78	31.11	30.31	31.62	30.70	32.16	29.27	25.57

	Scene	9	10	11	12	13	14	15	16
Bayer reconstruction	R	29.80	28.80	30.42	30.49	29.73	29.90	29.46	30.80
	G	29.97	29.39	30.19	30.27	30.04	30.17	30.14	30.33
	B	29.61	28.72	30.06	30.61	30.27	29.87	30.34	30.79
	RGB	29.79	28.96	30.22	30.45	30.01	29.98	29.96	30.64
Proposed method	R	31.93	30.18	32.44	32.57	30.90	31.71	30.45	32.30
	G	33.13	31.00	33.33	33.90	32.71	32.26	32.74	33.21
	B	31.77	30.28	31.99	32.64	32.03	31.72	31.95	32.38
	RGB	32.24	30.47	32.55	33.00	31.81	31.89	31.60	32.61

	Scene	17	18	19	20	Average
Bayer reconstruction	R	31.28	29.51	30.97	27.42	29.22
	G	30.57	30.00	30.47	29.21	29.76
	B	31.33	30.14	31.15	27.31	29.42
	RGB	31.04	29.87	30.85	27.90	29.44
Proposed method	R	33.36	30.77	32.09	31.07	30.96
	G	34.62	31.25	30.82	32.16	31.93
	B	33.38	31.87	31.69	30.95	31.34
	RGB	33.75	31.28	31.50	31.36	31.38

In Equation (10), S is the maximum pixel value, e.g., 255 for 8-bit images. Here, N is the total number of pixels in all frames. The value $\mathbf{f}_{true}(x,y,t)$ is the pixel value at position (x,y) of the time t reference image, and value $\mathbf{f}_{calc}(x,y,t)$ is the result of reconstruction.

We compared our method with the Bayer reconstruction [1,2,7-10,13,20] because they both use the same color filter array. Sensing images $\mathbf{g}$ are simulated by sampling the $\mathbf{f}_{true}$. We add the noise to $\mathbf{g}$ to be reflected during low

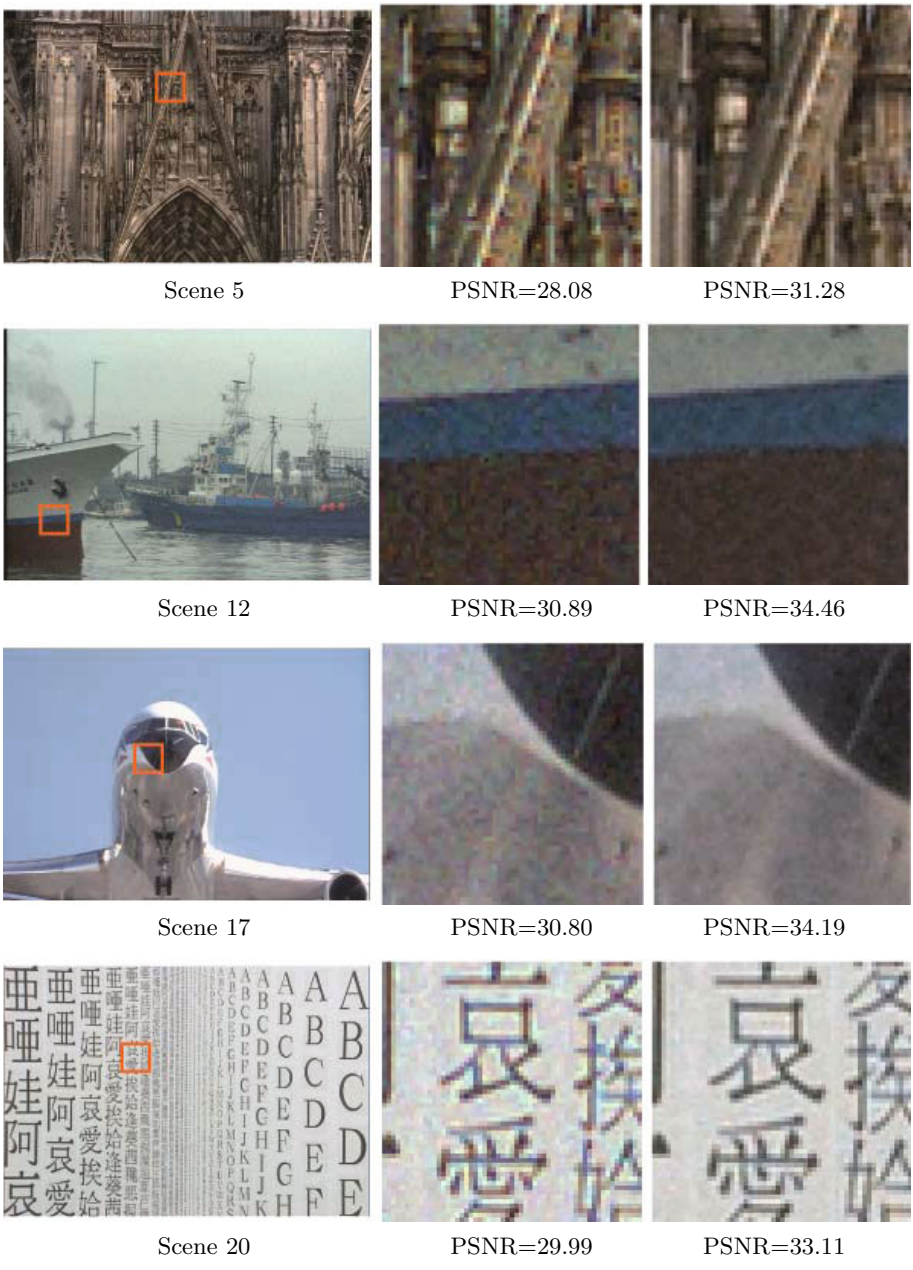

Fig. 4. (left) Test image sequences. (middle) Results of Bayer reconstruction and PSNR of picture area. (right) Results of proposed method and PSNR of picture area.

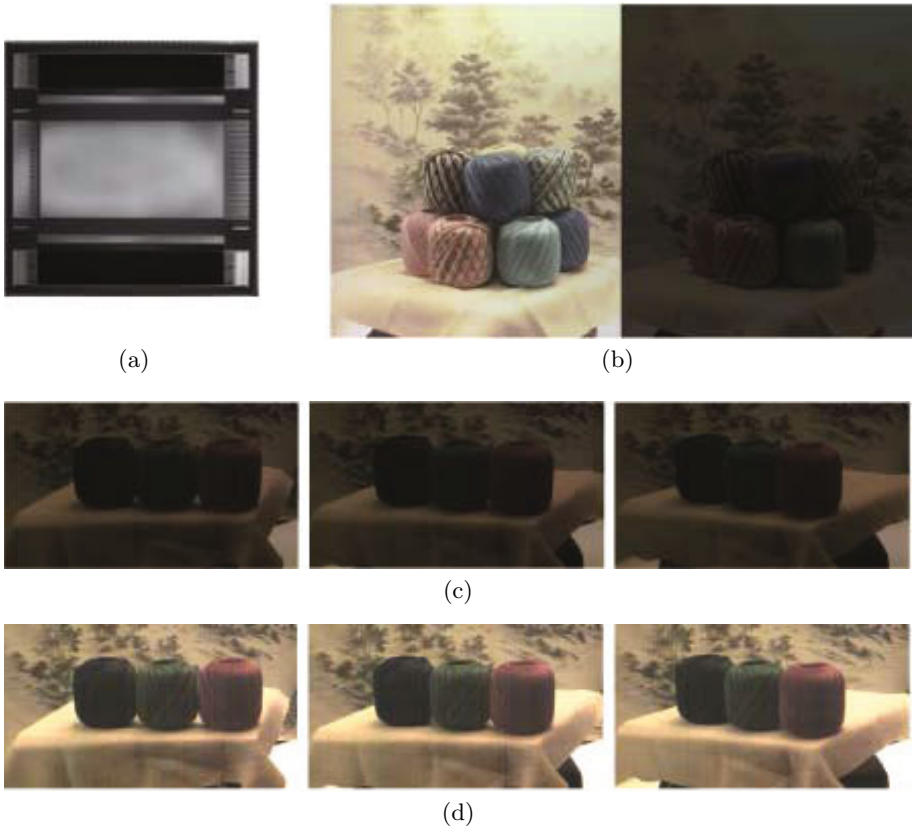

Fig. 5. (a) Image sensor used in proposed method. (b) Proposed method imaging and normal imaging. Proposed method uses long-term exposure for four frames. (c)Normal imaging sequence. (d) Proposed method imaging sequence.

illumination sensing. A long-term exposed image is defined as the sum of multi-frame images in **g**. The experimental conditions are listed in Table 1, and Table 2 and Figure 4 show the results of the experiment.

4.2 Development of Dedicated Image Sensor

We developed a dedicated image sensor to provide experimental proof. The single-chip image sensor is shown in Figure 5(a) and the results of using the sensor are shown in Figure 5(b)-(d).

The image sensor is 4K2K CMOS image sensor and was fabricated using a 0.25-μm process. The 4K2K pixels composed of three transistors and a photo-diode are arranged in a Bayer pattern. The transfer gates in the R/B and G pixels are connected with the different row lines, respectively. To reduce the operation frequency, the vertical shift register drives two rows of pixels through the

multiplexer, which applies readout pulses, respectively. This circuit configuration enables the R/B and G pixels to the addressed independently.

5 Discussion

The simulation results showed that the PSNR of our method was about 2 dB higher than that gained with Bayer reconstruction. Furthermore, our proposed method worked effectively in low illumination conditions.

The PSNR changes for each scene because the motion detection accuracy differs. If the motion of the pixels are spatially smooth, the detection accuracy will be high because the proposed sensing method interpolates motion information of long-term exposed pixels. The simulation results of scene 17, which is depicted in Figure 6(a) show that the PSNR is the highest of the 20 scenes. Because the

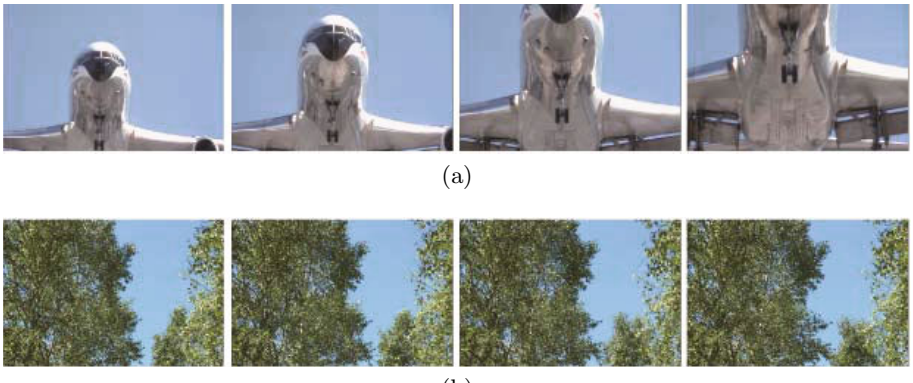

(a)

(b)

Fig. 6. (a) Images of 30 frame intervals in scene 17. (b) Images of 30 frame intervals in scene 8.

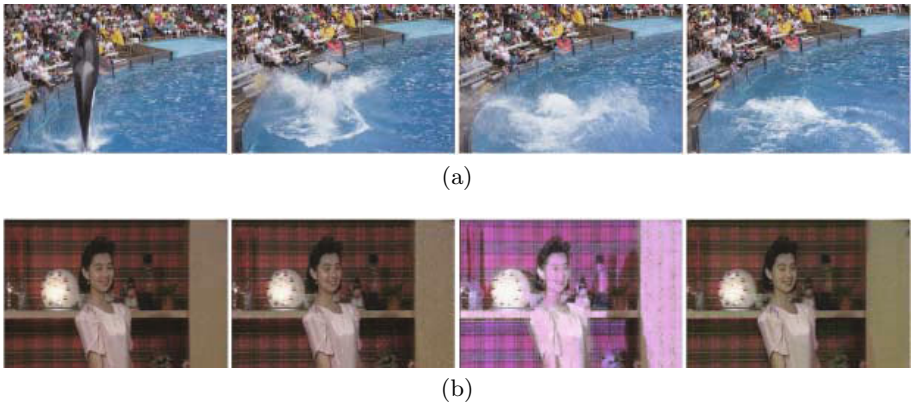

(a)

(b)

Fig. 7. (a) Image sequence of scene 7. (b) Images sequence of scene 19.

scene 17 dominatly contains spatially smooth motions. On the other hand, as shown in Figure 6(b), for scene 8, the PSNR is the lowest of the 20 scenes. Because the scene 8 contains large of variety motions. The differences in the PSNR of our method and that of the Bayer reconstruction are small in scene 7 and scene 19. We think that one reason for this is that the accuracy of the motion detection of these scenes is low. As shown in Figure 7(a), for scene 7, the motion of both the dolphin and the spray of water is large. As shown in Figure 7(b), for scene 19, the value changes greatly between consecutive frames because the light sometimes flashes.

The super-resolution processing adapts from a low-resolution image sequence to a high-resolution image sequence. This method requires either motion of the object or motion of the camera. Because our method does not need either of these terms, it is more effective than the super-resolution processing.

As shown in Figure 5(b), because our method uses long-term exposure for four frames, sensitivity is increased by four times.

6 Concluding Remarks

We proposed the image reconstruction method and its dedicated sensor for high-sensitivity imaging. Experimental results showed that our proposed method is effective in conditions of low illumination. We developed a dedicated single-chip image sensor and increased the imaging sensitivity fourfold.

Acknowledgement. This work was supported in part by National Institute of Information and Communications Technology(NICT).

References

1. Adams Jr., J.E.: Design of practical color filter array interpolation algorithms for digital cameras. In: Proc. SPIE, vol. 3028, pp. 117–125 (1997)
2. Adams Jr., J.E.: Interactions between color plane interpolation and other image processing functions in electronic photography. In: Proc. SPIE, vol. 2416, pp. 144–151 (1995)
3. Agrawal, A., Gupta, M., Veeraraghavan, A., Narasimhan, S.G.: Optimal coded sampling for temporal super-resolution. In: IEEE Conference on Computer Vision and Pattern Recognition (2010)
4. Bayer, B.E.: Color imaging array. US. Patent 3, 971, 065 (1976)
5. Nayar, S.K., Ben-Ezra, M.: Motion-based motion deblurring. IEEE Transactions on Pattern Analysis and Machine Intelligence 26(6), 689–698 (2004)
6. Bascle, B., Blake, A., Zisserman, A.: Motion Deblurring and Super-Resolution from an Image Sequence. In: Buxton, B.F., Cipolla, R. (eds.) ECCV 1996. LNCS, vol. 1065, pp. 573–581. Springer, Heidelberg (1996)
7. Cok, D.R.: Signal processing method and apparatus for producing interpolated chrominance values in a sampled color image signal. US Patent 4, 642, 678 (1987)
8. Hamilton Jr., J.F., Adams Jr., J.E.: Adaptive Color Plan Interpolation in Single Sensor Color Electronic Camera. US Patent 5, 506, 619 (1996)

9. Hamilton Jr., J.F., Adams Jr., J.E.: Adaptive color plane interpolation in single sensor color electronic camera. US Patent 5, 629, 734 (1997)
10. Hibbard, R.H.: Apparatus and method for adaptively interpolating a full color image utilizing luminance gradients. US Patent 5, 382, 976 (1995)
11. Honda, H., Iida, Y., Egawa, Y., Seki, H., Tanaka, N.: High Sensitivity Color CMOS Image Sensor with White-RGB Color Filter Array and Color Separation Process Using Edge Detection. In: International Image Sensor Workshop, pp. 263–266 (2007)
12. Iwabuchi, S., Maruyama, Y., Ohgishi, Y., Muramatsu, M., et al: A Back-Illuminated High-Sensitivity Small-Pixel Color CMOS Image Sensor with Flexible Layout of Metal Wiring. In: International Solid-State Circuits Conference, pp. 302–303 (2006)
13. Laroche, C.A., Prescott, M.A.: Apparatus and method for adaptively interpolating a full color image utilizing chrominance gradients. U.S.Patent 5, 373, 322 (1994)
14. Luo, G.: Color filter array with sparse color sampling crosses for mobile phone image sensors. In: International Image Sensor Workshop. pp. 162–165 (2007)
15. Popovic, Z.D., Sprague, R.A., Neville Connell, G.A.: Technique for monolithic fabrication of microlens arrays. Applied Optics 27(7), 1281–1284 (1988)
16. Rav-Acha, A., Peleg, S.: Two motion-blurred images are better than one. Pattern Recognition Letters 26(3), 311–317 (2005)
17. Rhodes, H., Tai, D., Qian, Y., Mao, D., et al.: The Mass Production of BSI CMOS Image Sensors. In: International Image Sensor Workshop, pp. 27–32 (2009)
18. Tai, Y., Du, H., Brown, M., Lin, S.: Image/Video Deblurring Using a Hybrid Camera. In: IEEE Conference on Computer Vision and Pattern Recognition (2008)
19. Wakabayashi, H., Yamaguchi, K., Okano, M., Kuramochi, S., et al.: A 1/2.3-inch 10.3Mpixel 50 frame/s Back-Illuminated CMOS Image Sensor. In: International Solid-State Circuits Conference (2010)
20. Weldy, J.A.: Optimized design for a single-sensor color electronic camera system. In: Proc. SPIE, vol. 1071, pp. 300–307 (1988)
21. Wuu, S.G.: BSI Technology with Bulk Si Wafer. In: International Image Sensor Workshop Symposium on Backside Illumination of Solid-State Image Sensors, pp. 124–153 (2009)
22. Yuan, L., Sun, J., Quan, L., Shum, H.Y.: Image deblurring with blurred/noisy image pairs. In: International Conference on Computer Graphics and Interactive Techniques, vol. 26(3) (2007)